Capability of a Time-of-Flight Camera as a Hazard Detection and Avoidance Sensor for a Moon Exploration Microrover

By Kentaro UNO,[1)] Louis-jerome BURTZ,[2)] Marc HULCELLE,[3)] and Kazuya YOSHIDA[1)]

[1)]*Department of Aerospace Engineering, Tohoku University, Sendai, Japan*
[2)]*KK ispace Inc., Tokyo, Japan*
[3)]*Ecole des Mines de Saint-Etienne, France*

(Received June 21st, 2017)

This paper describes the specific principles for the implementation of a time-of-flight (ToF) camera in the Google Lunar XPRIZE competition rover as a hazard detection and avoidance sensor. Each frame from the ToF camera provides a 3D point cloud of the environment. It is calculated by precisely measuring the round-trip time that light takes to travel from the near-infrared emitter, to objects in the scene and back to the imager. First, we investigate the suitability of the camera system to withstand the launch and space environment and report the results of qualification tests: a vibration test, thermal vacuum test, and radiation test. Second, we focus on the critical optical performance under lunar illumination conditions for which we conducted several experiments. We present the rationale and implementation of the first improvement made to the commercial version of the sensor to better suit strong illumination conditions. The optical tests are necessary to verify that the quality of the 3D point cloud is sufficiently reliable for input into the hazard detection and avoidance algorithm and that this novel ToF technology is suitable for the mission requirements. Through this research, a terrestrial sensor is qualified and customized to provide the data quality capable of autonomous hazard detection and avoidance on the lunar surface.

Key Words: Lunar exploration rover, ToF camera, Optical filter, 3D imaging

Nomenclature

DSP	:	digital signal processor
HDA	:	hazard detection and avoidance
NRT	:	near-real-time
ROI	:	region-of-interest
SEE	:	single event effect
SNR	:	signal-to-noise ratio
TID	:	total ionizing dose
ToF	:	time-of-flight
P	:	density of acceleration [G^2/Hz]
f	:	frequency [Hz]
Φ_e	:	spectral irradiance [W/(m^2nm)]
V	:	luminous efficiency function
λ	:	wavelength [m]

1. Introduction

Mobile robots with wheel-based locomotion systems have demonstrated that they are key technologies for the exploration of the surface of celestial bodies such as the Moon or Mars. In parallel, Earth application robotic technologies are showing tremendous capabilities for miniaturization. Team HAKUTO, a participant in the Google Lunar XPRIZE, is developing innovative solutions to launch a lunar exploration microrover for a 14-day mission.[1)] The Space Robotics Laboratory supports this and future missions with research focusing on bridging planetary rover exploration and robotic miniaturisation. Such missions are always accompanied by many severe limitations regarding the mass budget, payload volume, power consumption, and communication bandwidth. Because of the relative proximity of the Moon, a human-in-the-loop operation strategy was chosen for a higher speed of exploration and more agile development. However, this teleoperation scheme includes a significant time delay and extreme bandwidth limitations. Taking into account the light round-trip time and processing, the design specification assumes a 5 s delay between sending a command and receiving acknowledgement. The bandwidth limitations mean that the human operator must navigate using low resolution, highly compressed images. To maximize the exploration capability and reliability, an autonomous on-board hazard detection and avoidance capability is strongly required. Without such a system, more traditional space exploration operation procedures are required with more time spent planning each movement command.

Time-of-flight (ToF) cameras are promising technologies for robot awareness systems. Current research is employing ToF cameras as the main depth sensors in applications ranging from industrial robot automation to mapping and video game motion estimation.[2–4)] Specifically, to meet lunar/planetary rover mission requirements, as exemplified by the HAKUTO mission, the following criteria were the main design choices as we surveyed the market for ToF cameras:

- Miniaturized size and low power consumption
- Dense 3D point cloud and 2D image data (for accurate hazard classification)
- Low system-level computational impact (a dedicated digital signal processor (DSP) is ideal)
- No moving parts or mechanisms (to resist the launch vibration environment)

For this work, we selected the Bluetechnix Sentis M100 camera, as shown in Fig. 1 (main characteristics: Table 1), and used the 3D point cloud it delivers to autonomously detect mission-

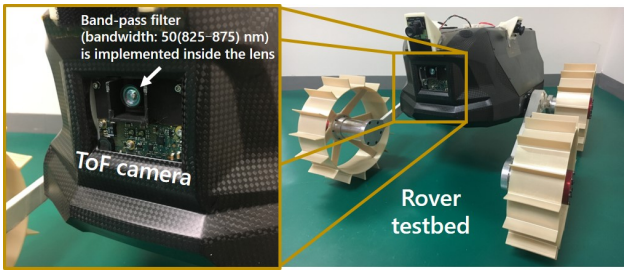

Fig. 1. Bluetechnix Sentis M100 camera attached to the rover testbed.

Table 1. Specifications of the Bluetechnix Sentis M100 camera.

Item	Unit	Value
Size	mm	$55 \times 42 \times 50$
Mass (without heat sink)	g	47
Average power	W	3
Imager	-	PMD Photonics 19k-s3
Resolution	pixel	160×120
IR peak wavelength	nm	850
Maximum frame rate	fps	40
Imaging range	m	0.1–3.0
Field of view	deg	90H × 60V
Operational temp. range	°C	(−40)–85
DSP	-	Dual 500 MHz Blackfin

critical boulders, slopes or ditches and immediately stop. So far, no such ToF pixel array technology has flown in space. A similar ToF device with a sensor of the same family is planned to be sent to the inside of the International Space Station (ISS) in 2017.[5] It will increase the autonomy of the Astrobee robot. In comparison with our mission, it will be exposed to similar vibrations during the launch but it will only operate in benign temperature and atmospheric pressure environment.

In this paper, we first report the hardware capabilities of such a novel sensor for surviving a journey to the Moon and the hostile conditions on its surface. We conducted three types of qualification tests to assess the viability of this sensor: a vibration test, thermal vacuum test, and radiation test. After these successful tests, the optical performance under a strong infrared (IR) flux became the single most critical risk before mission readiness could be proven. The second part of this paper presents the results from experiments under strong lighting conditions. Finally, we show an implementation of autonomous hazard detection and avoidance method using the ToF camera in a lunar microrover exploration mission context.

2. Qualification tests

2.1. Test objectives and procedures

We conducted component-level qualification tests. We present first the reason, conditions and procedure for each individual tests. The results are analyzed and compared together in Section 2.2 and Fig. 3.

2.1.1. Vibration test

The vibration test is critical to ensure that the sensor can withstand the launch environment. Following NASA guidelines,[6] we induced random vibrations at levels that model the rover loaded onto the lander in the rocket. Along three axes, the vibrations were measured to be 14.1 G_{rms}, where G_{rms} is the overall acceleration defined as Eq. (1). We confirmed that the hardware components of the ToF camera are not damaged through a functional power-on test between each axis of the vibration sequence. Then, back at the laboratory, we verified the the quality of the 3D point cloud through distance and amplitude measurements on calibrated surfaces and a compared the data with two untested reference ToF cameras (Section 2.2).

Table 2. Equilibrium conditions in the cold and hot environmental tests.

Test type	Hot test	Cold test
Item	Temperature [°C]	
Temperature of surroundings	40	-20
Vacuum chamber	41.8	-18.0
DSP main board	97	55
IR emitter board	80	38

$$G_{rms} = \sqrt{\int Pdf} \tag{1}$$

2.1.2. Thermal vacuum test

The thermal vacuum test demonstrates the conditions derived from lunar surface thermal simulations and vacuum conditions. The temperature range of the lunar surface during the HAKUTO mission is -19.6 °C to 43.8 °C, and our team implemented a full system thermal simulation.[7] Considering the results, thermal requirements, and operational temperature, we decided to use temperatures of -20 °C as the cold case condition and 40 °C as the hot case condition. The ToF camera is placed in a chamber with a constant environmental temperature. We set the integration time (2500 μs) and frame rate (5 fps) of the ToF camera as is expected during the mission. We measured the temperature of both the DSP main board and IR emitter board.

In both hot/cold cases, after about 120 min, the temperature of the device reached near equilibrium. Note: in the case of the hot condition test, true equilibrium was not achieved because the temperature of the DSP was about to exceed the predetermined 100 °C (Table 2) safety cut-off. We used the results from this test to inform the design of a new heat sink. With better thermal contact and a dedicated graphite sheet on the DSP, we reduce the temperature differential between the board and the environment.

2.1.3. Radiation test

The radiation test is the most challenging: the diversity in species, energy and flux (and their time variability) cannot be recreated. Simulation and modelling of the complex and highly integrated components is not satisfactory either. To address this challenge of representative conditions, we conducted two separate experiments: a single event effect (SEE) test using a proton beam and a total ionizing dose (TID) test by gamma ray irradiation.

The SEE test is to simulate high-energy particles (mostly solar energetic particles) and investigate the effect caused to IC by using fast protons accelerated by a cyclotron. Within the facility restrictions, we chose a representative energy and fluence for the beam parameters, as listed in Table 3. Monitored detrimental effects included:

- single event upsets (SEU): logic changes, usually recoverable through power cycling
- single event latchup (SEL) or single event induced burnout

(SEB): permanent damage due to short circuits or overcurrents induced by ionization events, non recoverable.

We experienced one single event upset that led to hanging of the ToF operating system. We stopped the beam, power cycled the device and started the experiment again, with no other problem noticed.

The TID test is representative of the aging of electronic components due to the accumulation of lower energy radiation. We determined the dose on the basis of simulations provided by the lander partner and the rate of exposure based on facility availability. The simulations take into account the radiation sources and their distributions along the Earth–Moon trajectory as well as lunar surface operations:

- 3.5 krad for the cruise phase (mainly due to the Van Allen belts) [device powered off]
- 0.4 krad for surface operations (uncertainty margin included) [device powered on and off repeatedly]

The dose is administered at three different rates. The first hour provides a dose of 3 krad, the second hour adds 7 krad, and the third hour adds 10 krad. The total dose administered represents a safety factor of five to mitigate the statistical resilience differences between each device. Note that the acceleration factor for the dose rate ranges between 60 for the first 3 krad/h exposure to 200 for the 10 krad/h exposure. This represents a deviation from the flight regime but is considered a stricter test.

2.2. Performance check

All ToF cameras passed the functional tests of booting and delivering a point cloud before and after each qualification test. After returning to the laboratory, we further confirmed the quality of the point cloud to detect more subtle degradations. The calibrated test setup used for all performance checks is shown Fig. 2. The test was carried out by comparing two untested reference ToF cameras against those that underwent qualification testing. We quantified the ability of the ToF camera to measure the distance accurately and determine the amplitude with identical sensitivity.

The results are shown in Fig. 3. There is no measurable deviation between the performance of the untested reference ToF cameras and the thermal-vacuum-, vibration-, TID-, and SEE-tested ToF cameras. However, there is a measurable deviation in the case of the total-dose-tested ToF camera; the amplitude is lower, and the distance is overestimated. The lower amplitude can be explained by aging of the sensor. The deviation in the distance measurement could be explained by an increase in the travel time of the signal in the ToF camera due to component aging, thus producing a higher distance estimate.

From a mission design standpoint, distance overestimation is critical to the hazard detection and avoidance algorithm. This knowledge is a critical parameter for the design of the keep out zone of the algorithm. Currently, the rover stops if any hazard is detected at a distance that is closer than 80 cm to the rover.

From the results and including the susceptibility to the TID, we concluded that the selected ToF camera is capable of functioning adequately once on the Moon and during the surface mission.

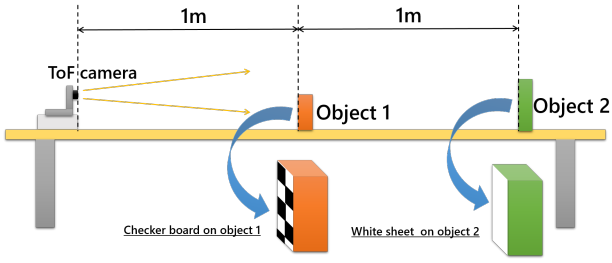

Fig. 2. Schematic of the performance checking test setup.

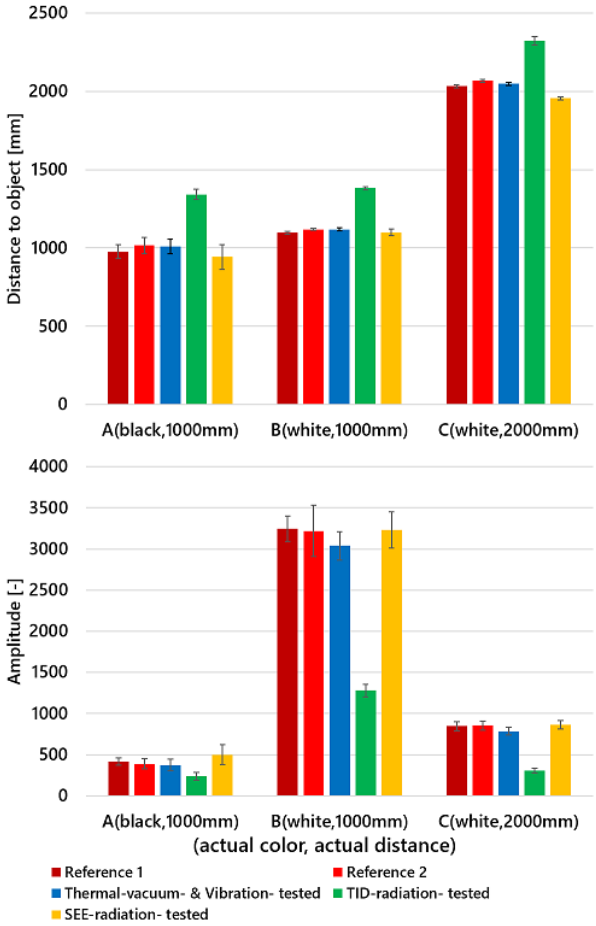

Fig. 3. Comparison of the distance and amplitude data obtained in the performance check test (error bars indicates ± standard deviation (σ)).

3. Optical capability under strong sunlight

3.1. Lunar optical environment

On the Moon's surface, the absence of an atmosphere allows for higher intensity sunlight to reach the surface. Today, the solar spectral irradiance is measured by an intelligent orbital spacecraft in detail, and ASTM International Standard E490-00a defines the "Standard Solar Constant and Zero Air Mass Solar Spectral Irradiance Tables," which list the spectral irradiance values for the range of 120–1000 nm.[8,9] By multiplying each wavelength with the standard luminous efficiency function from the International Commission on Illumination, the illuminance is calculated as shown in Eq. (2). On the basis of the ASTM standard, the calculated solar illuminance is 1.3 $\times 10^5$

Table 3. SEE beam parameters and the test results.

Energy [MeV]	Flux [cnt/(cm^{2}s)]	Fluence [cnt/cm^2]	Equivalent lunar surface time [days]	SEE occurrence
70	1.98×10^4	2.36×10^7	2.37	1 SEU
40	2.37×10^4	2.39×10^7	2.77	None

lux. Furthermore, particularly for the ToF camera, the near-infrared component of the external signal is critical because it can saturate the sensor pixel which makes the distance calculation impossible (no more phase information of the modulated light). Considering the range of 825–875 nm, the solar irradiance is 4.8 mW/cm^2 by integrating the ASTM spectral irradiance data.

$$\Phi_v = 683.002 \times \sum_{\lambda=380}^{780} \Phi_e(\lambda)V(\lambda)\Delta\lambda \qquad (2)$$

3.2. Effect of strong sunlight

The ToF camera used was also chosen for the specific photonic mixer detector (PMD) technology that it implements. For increased robustness against sunlight, this depth sensing technology relies on the time-of-flight of modulated light instead of other approaches like structured light. The structured light approach projects a known IR pattern on the scene and the IR sensitive sensor detects the deformation of this pattern to compute distance (used for instance in the Microsoft Kinect). In this approach, the projected light must have higher power when it reaches the object than the natural IR light reflected on the object by other sources (mainly sun). Understandably, the performance is greatly reduced in any outdoor setting.

On the other hand, the time-of-flight technology computes the distance from the camera to the object by precisely timing the round trip of the emitted light by the illumination LEDs hitting the object and returning back to the sensor. Among other things, this allows for using modulated light. In the PMD technology, 20 MHz modulated light is used and patented circuitry (suppression of background illumination circuitry) at the pixel level eliminates all contribution from light that is not correlated to the specific LED illumination frequency.[10)]

However, even with this technology, we observe that under strong sunlight illumination, an important drop in signal-to-noise ratio (SNR) is produced, as shown in Fig. 4. In the left image which color-codes the calculated distance, we observe many pixels with absurd values where the ground and the obstacle should be. We also observe ghost pixels in the upper part of the field of view, where no physical object is present. In the right image which shows the amplitude values (the amount of modulated IR light received), we observe black points that correspond to invalid or saturated pixels.

The correlation between the invalid/saturated pixels and absurd distance measurements means that noise from the sun exceeded the suppression of background illumination capability of the pixels. Being saturated by the noise from the Sun, no distance measurement based on the emitted light from the ToF is possible.

We therefore understand that the main reason for this data quality drop is the saturation of the pixels. We know the pixels are sensitive in the range of 650−1200 nm (corresponds to over 10% relative spectral sensitivity). However, the ToF emitters are IR LEDs with a central wavelength of 850 nm and a

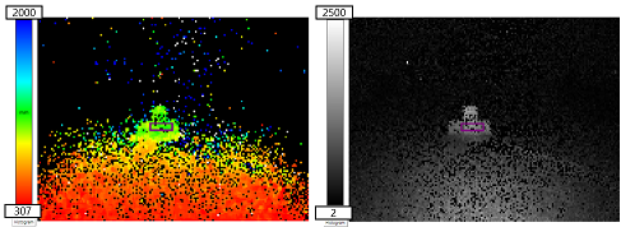

Fig. 4. color-coded representation of distance (left), and 2D gray scale image of amplitude (right).

full width at half median of only 30 nm. Therefore, there is no useful signal outside of the 825−875 nm band, but only the potential for noise from the sunlight. In other words, over the sensor sensitivity band, the sun outputs significant power and drowns the useful signal from the ToF camera's emitters. A 50 nm band-pass filter centered on 850 nm wavelength is therefore an ideal candidate to reject as much as possible of the IR component from the sun and increase the SNR of the point cloud.

3.3. Effect of a hardware band-pass filter

To make the most of the selected ToF camera ' s abilities, a band-pass filter was implemented behind the lens immediately above the sensor, as shown in Fig. 1. To investigate how critical to the quality of the 3D point cloud a strong external light is, and evaluate the effectiveness of the band-pass filter, we conducted an outside test on a clear day (Fig. 5). Pictured on the right side is the mechanical mount that held the ToF cameras in the same orientation and at the same height above the ground as when mounted on the lunar microrover. The two side by side cameras captured the data simultaneously: one has the band-pass filter, the other is a non-customized reference ToF camera. A luxmeter used to monitor the direct incoming sunlight completed the test setup.

The illuminance values and the resulting 3D point cloud data obtained by hardware filter/no-filter ToF cameras are shown in Table 4 and Fig. 5. The data was taken under illumination conditions always above 10^5 lux.

Standard deviation is used as a data quality observable: it quantifies both the spatial variability of the measurements across the surface of the object (9×4 pixels) and the repeatability of the measurement in time (30 frames). The standard deviation measurements of the hardware filter ToF camera are always significantly lower than the no-filter ToF camera (Table 4). This is true both for the amplitude and the distance measurements.

The visualisation of the full 3D point cloud also yields new insight on the quality improvement made possible by the hardware filter (Fig. 5). Without the hardware filter, the number of noise dominated points with absurd 3D coordinates is significantly higher. With the hardware filter, both the 500 μs and the 1000 μs settings yield acceptable point cloud quality.

3.4. Night field test with controlled lighting conditions

To investigate the effect of direct spot sunlight and verify the performance of our ToF camera to detect a hazard, we conducted a field test in the Tottori sand dunes (Fig. 7). We con-

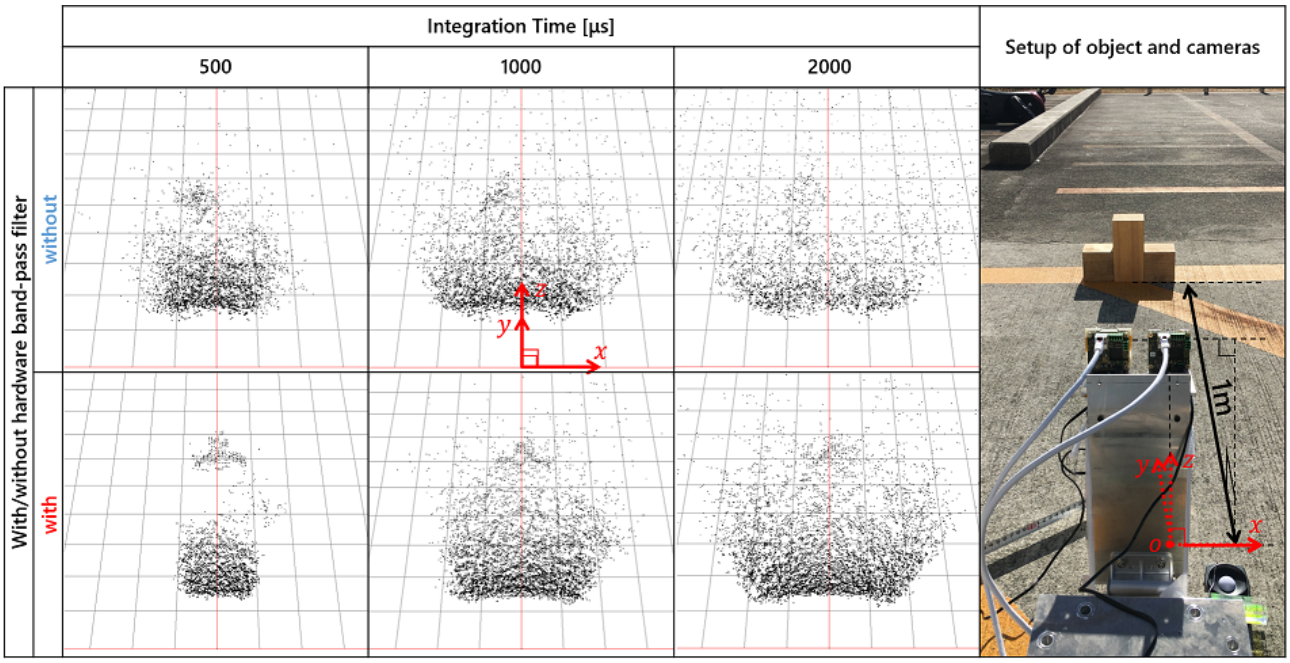

Fig. 5. 3D point cloud data obtained by the reference and hardware filter ToF cameras as a function of integration time.

Table 4. Standard deviation (σ) values obtained by changing the integration time with the reference and the hardware filter ToF cameras (each σ were calculated by using 1080 pixels: (9 × 4) pixels × 30 frames).

With the hardware band-pass filter	Illuminance [lux]	Integration time [μs]	Standard deviation (σ) of distance	Standard deviation (σ) of amplitude
No	1.14×10^5	500	52.6	113.8
Yes	1.14×10^5	500	30.6	80.9
No	1.10×10^5	1000	44.0	397.1
Yes	1.10×10^5	1000	26.2	188.3
No	1.08×10^5	2000	541.4	1034.1
Yes	1.08×10^5	2000	26.0	664.3

ducted this test during the night, to avoid the variability and the non-directionality (atmospheric diffusion) of natural sunlight. In this test, the ground surface and obstacles are illuminated by an HMI lamp and a spot lens. The setup provides near collimated light and is directed with the worst case sunlight angle expected during the mission: 30 degrees. Our experiments were performed under high illuminance values, as determined by the same lux-meter and logged in Fig. 8. Under these conditions, the ToF camera equipped with the band-pass filter could capture strikingly more accurate 3D point cloud data than the no-filter one. From Fig. 9, we confirmed the following important facts.

- The strong spot illumination causes a new type of noise that we are naming a ghost region-of-interest (ROI) (seen on the left side of Fig. 6 or bottom right of Fig. 9). We interpret this phenomenon as analogous to lens flare (successive reflections in the lens assembly)
- The band-pass filter significantly decreases the noise in the data, and reduces the extent of the ghost ROI (Fig. 6)
- The ToF camera can accurately detect obstacles that are located up to 1.5 m away

3.5. Summary

Regarding the optical capability under strong sunlight, we verified that the band-pass filter concept can improve the SNR at a given integration time. Furthermore, because the range directly depends on the integration time, this improvement translates to either:

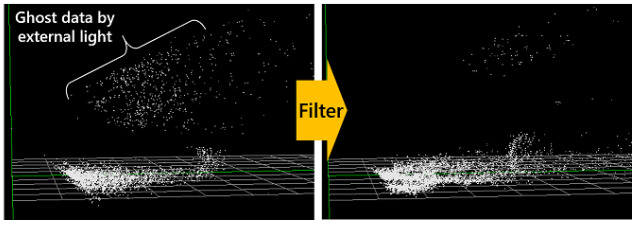

Fig. 6. Side view of the 3D point cloud taken by no-filter and hardware filter ToF cameras.

- better point cloud quality at a given range
- longer range for a given point cloud quality

These experiments under strong sunlight also confirms that the expected detection range on the Moon is obviously less than that for indoor applications. For the rover, the requirement is accuracy up to 1−2 m in front of the rover. This will allow the hazard detection algorithm to identify obstacles and issue the emergency stop signal with sufficient safety margin.

4. Implementation of the emergency stop system

Using reliable 3D point cloud data, it is possible to create an emergency stop function. In a related work, object classification by ToF cameras was reported and is the basis of the haz-

Fig. 7. Overview of the Tottori analog lighting test

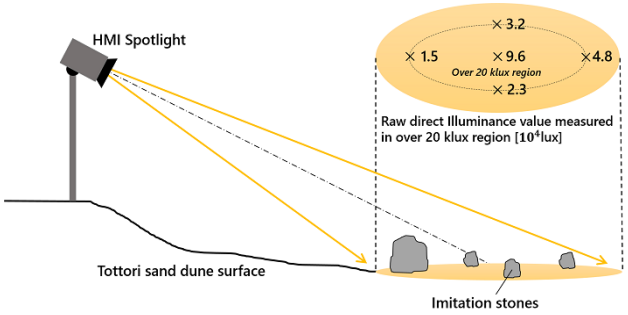

Fig. 8. Schematic of the Tottori field test under the analogue lighting environment.

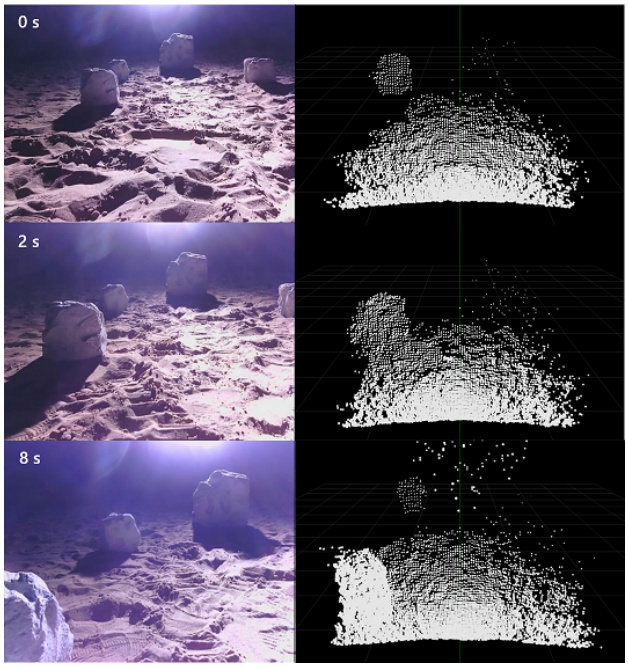

Fig. 9. NRT pictures (left) and 3D point clouds (right) obtained during the Tottori field test. (ToF camera's integration time: 2500 μs)

ard detection and avoidance algorithm implemented in this research.[11] In our mission context, to maximize the safety during exploration, we suggest a combination of human teleoperation and autonomous emergency stops, as shown in Fig. 10. A human operator sends movement commands of no more than 1 m at a time. During movement, the front visible-light camera captures images. However, due to severe bandwidth limitations, the human operator can only visualize them at 1 frame per second, heavily compressed and with a delay of around 5 s : conditions

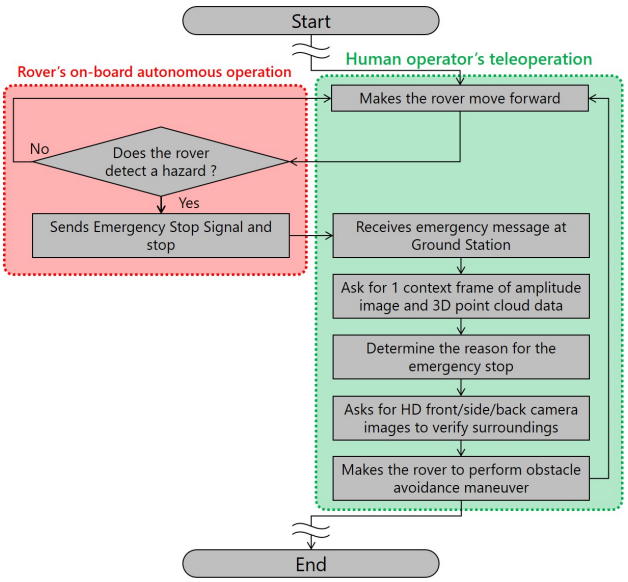

Fig. 10. Flowchart of proposed hazard detection and avoidance method.

dubbed near-real-time (NRT). As soon as a hazard is detected by the algorithm, an emergency stop signal is sent and it autonomously stops the rover. Additionally, the characteristics and location of the hazards are continuously sent to the ground station. The human operator can also request HD pictures taken by visible-light cameras on the four sides of the rover. Finally, the operator can use the combination of this information to update the rover route to a safer path.

We developed a prototype of the emergency stop algorithm and conducted initial experiments in Sendai beach, Japan. The location is chosen for its lack of vegetation and fine sand to provide an unstructured environment comparable with the lunar surface. The basic procedure of hazard detection and avoidance (sending an emergency stop signal) is as follows:

1. Recognize the flat ground surface in front of the rover. It is considered safe and removed from further computation.
2. Detect a ROI either over the ground (gravel, boulder or slope) or under the ground (ditch) and compute their 3D characteristics.
3. If a boulder or a ditch is detected less than 0.8 m in front of the rover, an automatic emergency stop signal is sent to the rover wheels.

In these dynamic experiments, we tested three main hazards: a boulder, slope and ditch, as shown in Fig. 11. As a result, in every case, the emergency stop signal was sent successfully (Fig. 12). From the bird's eye view images, we observe that the rover always stopped once the hazard came within 0.8 m.

However, an important number of false positives were sent: the emergency stop command was sometimes sent even if there was no hazard (as judged by a human eye). False positives are less mission critical than false negatives, but they slow down the exploration.

We also realized that the ground level suppression process removes too much data and induces errors in the hazard detection. Further work is required regarding the parameters related to detection of the ground and the thresholds for hazards to be considered dangerous.

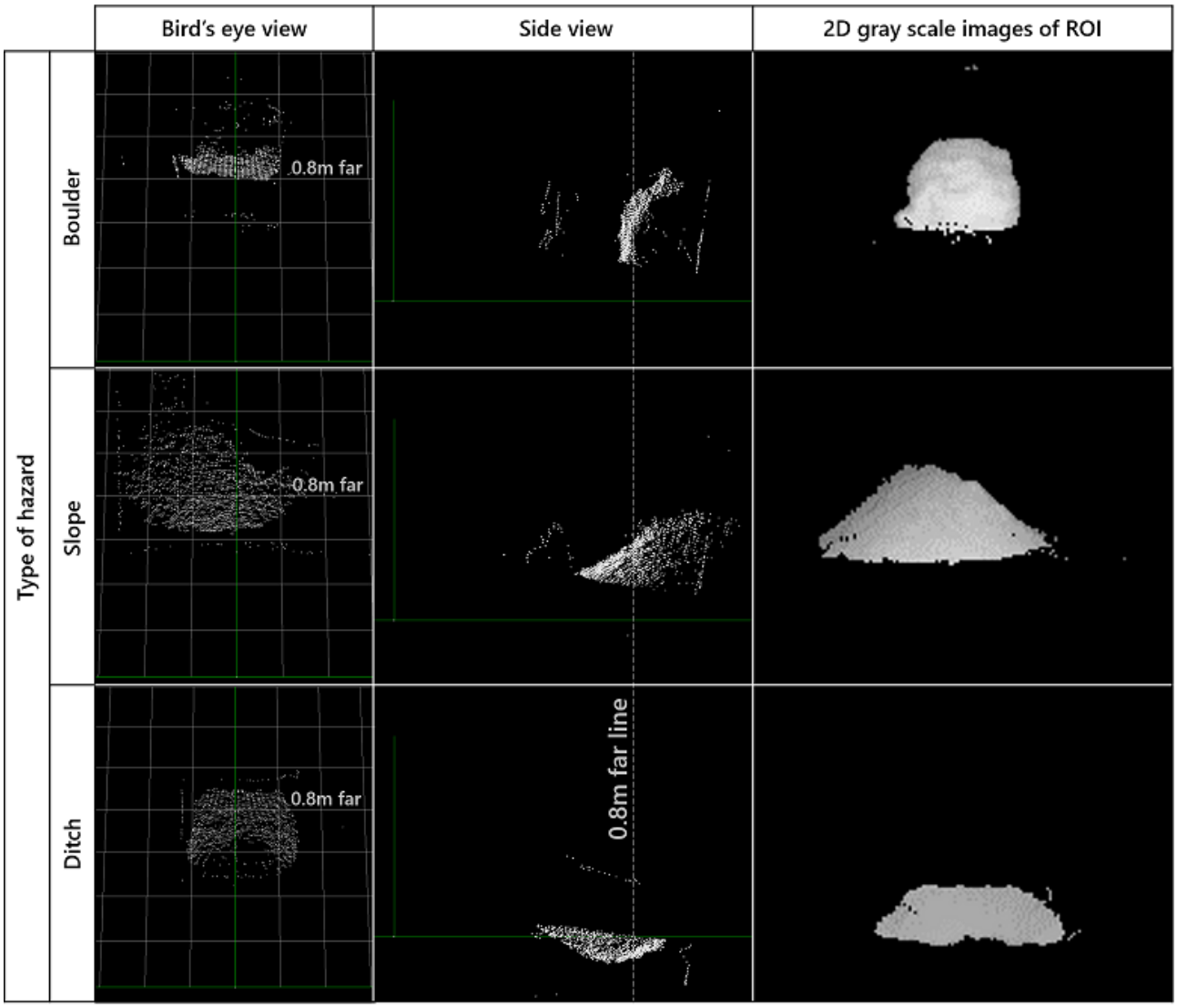

Fig. 12. Obtained 3D point clouds and 2D amplitude images (ToF camera's integration time: 700−1000 μs)

Fig. 11. Overview of the emergency stop algorithm trial experiment at Sendai beach.

5. Conclusion

First, from the results of the qualification tests and subsequent performance analysis, we conclude that the mechanical viability of the selected ToF camera meets the lunar mission requirements. Second, through the optical demonstration test, we find that the lunar illuminance and irradiance cause noise in the 3D point cloud data taken by the ToF camera, but it is possible to increase the SNR with a band-pass filter. Finally, we verified how to use the ToF camera's 3D data to create an emergency stop signal necessary for reliable lunar/planetary exploration. From this research and pending future work, we conclude that the ToF camera has high potential as a hazard detection and avoidance sensor for planetary exploration rovers.

For future work, we are building on the demonstrated potential of the band-pass filter customization with plans this time to change the LED emitters to laser diodes. This will permit two significant improvements: being able to increase the optical power (increase the signal) and further reduce the bandwidth of the filter (reduce the noise).

In parallel, we plan to develop a software filtering algorithm to decrease the error and noise in the point cloud before it is sent to the main HDA algorithm. Software filtering within each frame and in between successive frames will be explored. A strong requirement will be to keep the computational loads low enough for continued real time processing.

During each field test presented above, raw point cloud data

was also collected and provides a database that will be further analyzed and used to efficiently test improvements to the HDA algorithm.

Our final aim is to provide gradual research to advance the use of time-of-flight technology for environment perception in miniaturised rovers, for applications both on Earth and other celestial bodies.

Acknowledgments

We express our special thanks to Ms. Alix Ollivier and Mr. Sebastian Karl Henrik Nilsson for their considerable efforts to develop on-board emergency stop algorithm and to embed the software onto the ToF camera's DSP.

References

1) Walker, J., Britton, N., Yoshida, K., Shimizu, T., Burtz, L., and Pala, A.: Update on the Qualification of the Hakuto Micro-Rover for the Google Lunar X-Prize, Proceedings of the Field and Service Robotics Results of the 10th International Conference, Toronto, Canada, 2016, pp.313–330.
2) Alenyà, G., Foix, S., and Torres, C.: ToF Cameras for Active Vision in Robotics, *Sensors and Actuators A: Physical*, **218**, 2014, pp.10–22.
3) Almansa-Valverde S., Castillo, J. C., and Fernández-Caballero, A.: Mobile Robot Map Building from Time-of-Flight Camera, *Expert Systems with Applications*, **39, 10**, 2012, pp. 8835–8843.
4) May, S., Fuchs, S., Droeschel, D., Holz, D., and Nüchter, A.: Robust 3D-Mapping with Time-of-Flight Cameras, Proceedings of the IEEE/RSJ International Conference on Intelligent Robots and Systems, 2009, St. Louis, USA, pp.45–55.
5) Smith, T., Barlow, J., Bualat, M., Fong, T., and Provencher, C., Sanshez, H., Smith, E., and the Astrobee Team: ASTROBEE: A New Platform for Free-Flying Robotics on the International Space Station, *NASA Technical Reports Server*, ARC-E-DAA-TN31584, 2016, USA.
6) General Environmental Verification Standard (GEVS) for GSFC Flight Programs and Projects, Goddard Technical Standard, 2005, pp.68.
7) Oikawa, T., Tanaka, T., Walker, J., Uno, K., Costa, P., Britton, N., and Yoshida, K.: Thermal Design and Analysis of Conceptual Flight Model for a Lunar Exploration Rover, Proceeding of the The International Symposium on Artificial Intelligence, Robotics and Automation in Space, ,Beijing, China, 2016.
8) Thuillier, G., Hersé, M., Labs, D., Foujols, T. Peetermans, W., Gillotay, D., Simon, P.C., and Mandel, H.: The Solar Spectral Irradiance from 200 to 2400 nm as Measured by the SOLSPEC Spectrometer from the Atlas and Eureca Missions, *Solar Physics*, **214**, 2003, pp.1–22.
9) ASTM: Standard Solar Constant and Zero Air Mass Solar Spectral Irradiance Tables, Active Standard ASTM E490, ASTM E490-00a, **15.03**, 2014.
10) Mller, T., Kraft, H., Frey, J., Albrecht, M., Lange, R.: Robust 3D Measurement with PMD Sensors, Proceedings of the 1st Range Imaging Research Day at ETH, Zurich, Switzerland, 2005.
11) Yu, H., Zhu, J., Wang, Y., Sun, M., and Tang, Y.: Obstacle Classification and 3D Measurement in Unstructured Environments Based on ToF Cameras, *Sensors*, **14, 6**, 2014, pp.10753–10782.